Development and Characterisation of Completely Degradable Composite Tissue Engineering Scaffolds

PhD Thesis by Montse Charles-Harris Ferrer

PhD Supervisor: Josep A. Planell i Estany

Barcelona, July 2007

Chapter 7: Synchrotron X-Ray Microtomography and in-situ micromechanical testing of solvent cast scaffolds.

Foreword

The European Synchrotron Radiation Facility (ESRF) in Grenoble, France, allocates its beam time upon application. Our first proposal for beam time was accepted and we obtained 15 shifts in September 2004 to perform X-ray microtomography and in-situ micromechanical testing of our composite scaffolds. At the time, we had only developed the solvent cast scaffolds. None of our following proposals were accepted before the completion of this PhD thesis, thus we have not been able to characterise the phase-separated scaffolds. Beam-time was eventually allocated for our proposal in February 2007. Thus the phase-separated scaffolds with optimised compositions were characterised at the ESRF but are not included in this thesis.

Introduction

An ideal tissue engineering scaffold should offer appropriate mechanical, structural, chemical, and surface properties. Thus, a thorough characterisation of the scaffolds is crucial in order to assess their suitability and to understand the biomechanical environment the cells will sense upon seeding. As has been seen in previous chapters, however, the characterisation of these highly porous biomaterials is not straightforward since they often fall out of the scope of traditional materials tests or cell culture studies. Thus, characterising certain aspects of scaffolds such as mechanical properties and achieving results which can be easily compared between different authors remains a challenge. This chapter explores the potential of synchrotron X-ray microtomography as a tool in tissue engineering scaffold characterisation which could help to solve some of the shortcomings of current testing methods. Beamline ID22 at the ESRF was used to obtain microtromographies and simultaneous in-situ micromechanical tests of the scaffolds.

A synchrotron is a particle accelerator. Particle accelerators are all based on the interaction of the electric charge with static and dynamic electromagnetic fields. They can be linear or circular, and always contain two basic units: a particle source or

injector, and the main accelerator. Different particle sources such as glow discharge columns or cathodes are used to produce the variety of particles that can be accelerated: protons, ions, antiprotons, electrons and positrons. The particles are generated as a continuous stream of particles which must often be compressed into a shorter pulse with a chopper device and a prebuncher. The chopper can be a mechanical device, a deflecting magnet, or a radio frequency field moving the beam across the opening of a slit. The beam then exits the chopper in the form of pulses called bunches.

A linear accelerator consists of a series of accelerating fields timed such that particles absorb and accumulate energy from each accelerating unit. For very high beam energies, linear accelerators become very long and costly. These problems can be avoided in circular accelerators where the beam is held on a circular path by magnetic fields in bending magnets. The beam passes repeatedly at every turn through accelerating sections, similar to those in linear accelerators. In this case, the particles gain energy from the accelerating cavities and reach maximum energy when the fields in the bending magnets are raised in synchronism. Such circular accelerators are called synchrotrons.

An early limitation of circular particle accelerators was the energy lost when accelerating electrons. When electrons are accelerated to produce high density electron beams, they produce large amounts of synchrotron radiation. This synchrotron radiation, however, has proven useful for basic and applied research and technology. In order to implement synchrotron radiation, the particle beam is not maintained in constant acceleration. Instead, it is stored in orbit for several hours in storage rings. These storage rings are not particle accelerators in the strict sense, but are the base of most modern day synchrotron radiation facilities. The synchrotron radiation produced at the ESRF are extremely bright X-rays which can be applied to the study of very different research fields[1,2].

Synchrotron radiation allows for the in depth study of both the structural and electronic properties of matter due to its very intense and high quality brightness. Some examples of synchrotron radiation applications are: the analysis of the crystal structure of complex macromolecules, the changes in the structure of matter under different thermal and mechanical treatments, and the study of gas-liquid-solid interactions at interfaces or surfaces and high-resolution 3D tomographies. High-resolution 3D

tomography performed with synchrotron radiation has been used in this study to characterise the microstructure of the scaffolds.

The microstructure of tissue engineering scaffolds can be imaged using two-dimensional (2D) or three-dimensional (3D) microscopic techniques. 2D imaging is insufficient to assess some 3D characteristics such as porosity, pore interconnectivity or phase distributions within composite materials. Furthermore, some 2D techniques require transparent or translucent materials. Microtomography is a 3D non-destructive technique which provides isotropic data on material morphology. Synchrotron X-Ray microtomography offers high-resolution 3D images thanks to the monochromatic beam and the high photon flux (approximately 10^{12} photons/s).

Synchrotron X-ray microtomography has been used previously to perform thorough characterisations of biomaterial morphologies. It has been applied to evaluate the properties of hydroxyapatite coatings deposited on titanium surfaces using phase-contrast imaging[3]. Specifically, in the case of polymeric scaffolds, this technology has been applied to study the microstructure of porous Poly(D,L-lactic-co-glycolic) acid scaffolds[4,5]. The authors compare the accuracy of their 2D and 3D data in characterising the porosity and develop a methodology to quantify a mean pore diameter value.

Microtomography has also proven useful to assess cell-scaffold morphology after cell culture or implantation. It has been used to compare and quantify different degrees of bone in-growth at various implantation times in calcium phosphate cements[6-8]. Its 3D potential was exploited by Thurner et al.[9] to perform an elegant comparison between fibroblast and osteoblast-like cell growth on poly-ethyleneterephthalate yarns by using synchrotron X-ray imaging, addressing, in addition, the crucial issue of taking cell biology into the “third dimension”. Tuan et al.[10] use micro computed tomography to quantify porosity, interconnection and osteochondral repair in polycaprolactone meshes.

In addition to characterising the microstructure of the scaffolds, synchrotron X-ray microtomography can also be used to assess their mechanical behaviour. The mechanical properties of scaffolds are generally measured by means of their compressive properties. Compression is thought to be one of the prevailing loading modes they will experience in vivo[11]. Many authors have measured and discussed

these properties[12-14]. However, testing procedures described in the literature are generally incompletely defined and have been adapted from testing standards which are not always applicable[15-17]. This is due to the fact that sample dimensions are limited and the interpretation of the compression curves of these foamed materials is complex. Beamline ID22 at the ESRF has developed a tomopress to perform in-situ mechanical testing during the microtomographies, and thus obtain 3D images of the scaffolds under compression.

This study combines synchrotron X-ray microtomography with simultaneous in-situ mechanical tests to analyse the microstructure and the deformation of completely degradable composite scaffolds made by solvent casting. Three compositions of the scaffolds are imaged at different strains, in order to study the scaffolds' porosity, pore deformation under strain and the distribution of the glass within the polymeric matrix. Finally, the tomographical images are converted into a finite element mesh which will be used to evaluate the mechanical properties of the scaffolds numerically.

Materials and Methods

Materials

The scaffolds used for the microtomography experiment were made using the solvent casting method described in detail in Chapter 2. They were made with NaCl particles sieved between 80-210 μm, and glass particles measuring less than 40μm at 0 wt%, 20 wt% and 50wt%. SEM images of the tomographical samples were taken to ensure the scaffold microstructures were representative of the conventional samples (12mm diameter), and to compare with the tomographical images. Normal macroscopic compression tests were performed, as described in Chapter 2, to determine the strain levels applied during the in-situ mechanical tests.

Microtomography

The microtomography experiments were carried out at the ESRF at the micro-fluorescence, imaging and diffraction (μ-FID) beamline ID22[18]. The maximum

electron current was 200mA in uniform filling, and the source size from the high-beta section of the ESRF storage ring was 800×30μm (horizontally×vertically). The samples were mounted at a distance of 65m from the undulator source. Phase-contrast microtomography was performed with an energy of 17keV, at a distance of 20mm and with a 1s exposure time. The X-ray projections of the samples were recorded with a high-resolution CCD-based camera system. The scintillator screen was a LAG:Eu with a 3.5 μm luminescent layer. 875 phase-contrast images were recorded at equi-spaced angular rotations between 0° and 180°. 3D volumes were reconstructed from these sets of data using filtered-backprojection[19]. The resolution was 0.7 μm × 0.7 μm × 0.7 μm.

Phase-contrast imaging was used because of its applicability to investigate materials with very low X-Ray absorption such as polymers. This technique relates to the refractive index of the sample, and can thus reveal information about details of very thin objects or objects that are virtually transparent to X-Rays.

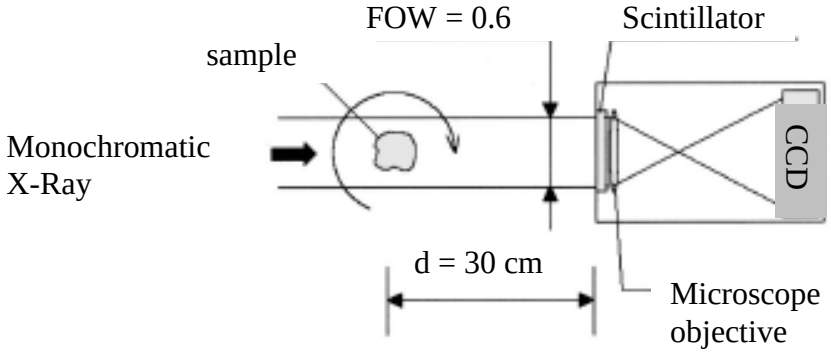

Figure 7.1: Microtomographical set-up of the sample and scintillator at beamline ID22 of the ESRF. (FOW stands for Field of View)

When imaging at high resolutions (0.7μm), the field of view of the X-ray detector is limited to 1.4 mm, which restricts the sample diameter to that value (Figure 7.2). Thus, the samples used for microtomography were cylindrical; and measured 1.2 mm in diameter and 3 mm in height.

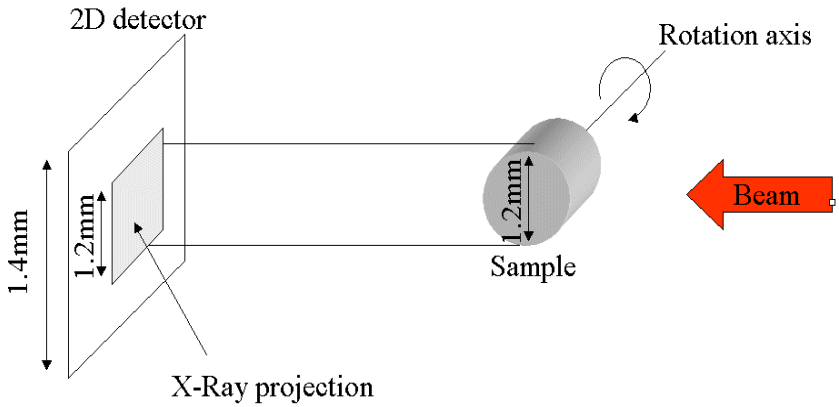

Figure 7.2: Schematic of the X-Ray projection of samples on the 2D detector

For conventional tomography, the samples were mounted onto brass goniometers. The in-situ micromechanical tests were performed using the microtomographical press available at beamline ID22[20]. The mechanical tests were performed in displacement-controlled compression.

Image treatment

The X-ray projections and radiographs were pre-treated using ImageJ and VGStudioMax software. Both binary and greyscale images were analysed. Mimics 8.11 (Materialise) software was used to quantify the phase distribution and porosity of the scaffolds. As Lin et al.[21] report, this software can be used to threshold the greyscale images and create masks. « Mask » is the term used by the software to designate a series of pixels that contain meaningful information. Thus masks can be created including all the pixels that represent the polymer, the glass particles and the pores, for example. The volume of the masks can in turn be used to calculate the porosity, surface/volume ratio and volume percent (Vol%) of PLA and glass in the scaffolds. Mimics 8.11 features a region-growing function. This function creates a mask containing all points connected to a marked point, thus a mask can be created by selecting a single point and making the programme add all other points connected to it. Thus a mask of a continuous phase can be created, or in the case of this study, a mask of the interconnected porosity can be created and the degree of pore interconnectivity can be quantified.

Finite Element Analysis

After image treatment, a cylindrical section (radius = 550μm, height = 140μm) of the 3D volume images was surface meshed into finite elements with Mimics and Magics (Materialise) software. The surface mesh, or shell, was corrected to avoid artifacts created by meshing the complex geometry. The surface mesh was then exported to the MSC Mentat pre-processor and meshed in volume with tetrahedral elements. Despite meshing only a small section of the scaffold volume the final 3D model contained more than 200,000 elements.

A linear elastic simulation of a compression test was performed on MSC Marc software in order to validate the model. A 5% strain was applied on the upper nodes of the model. The scaffold material was assumed to be an isotropic composite with 50 wt% of glass particles. The material was given a Young's Modulus, Y, of 3.5 MPa and a Poisson's ratio, ν, of 0.33. The value of the Young's modulus in compression of the porous solid, E_c, was derived from the following equation that states the relationship between the E in compression of a cellular solid and its porosity[22]:

$$E_c = Y \times (1 - P)^m \qquad \{1\}$$

where E_c= the Young's modulus in compression of the porous solid, Y= the Young's modulus of the non-porous solid, P= porosity, and m = a coefficient that varies between 1 and 3 and depends on the morphology and the orientation of the pores. Previous studies varying the porosity of the composite scaffolds (50 wt% of glass) between 75% and 95% gave a value of m of 0.8265 and of E_c of 3.5 MPa.

In addition to validating the model, the preliminary finite element results were analysed in order study the stress and strain distribution in the scaffold.

Results

X-Ray Microtomography and Image Treatment

Phase contrast microtomography was used due to the low X-ray absorption of the sample material. Tests using absorption mode gave very poor contrasted images. The X-ray radiographs of the samples at different compositions reveal the pore and glass particle distribution. Figure 7.4a shows the projection of a scaffold without glass particles, the thin pore walls can be seen forming a random though fairly regular net,

with evident interconnectivity. The projection of the scaffolds with 20wt% and 50 wt% of glass particles (Figure 7.4b,c) reveal the even distribution of the glass particles throughout the scaffold.

The in-situ compressive tests were quite challenging due to the small size of the samples (Figure 7.3). The scaffolds were placed horizontally between the grips using a mini-vacuum aspirator. A small amount of pre-strain had to be applied on the tomopress grips in order to maintain the scaffold in place. This pre-strain could not be calibrated. Six or seven strain levels were imposed for each scaffold, a complete microtomography was performed at each strain level. The projection at 20% strain on a sample with 50wt% of glass particles, shows pore-wall breakage which is especially evident on the sample surface (Figure 7.5b). At higher strain levels, the scaffolds suffer extreme compressive modes such as buckling and barrelling (Figure 7.5c).

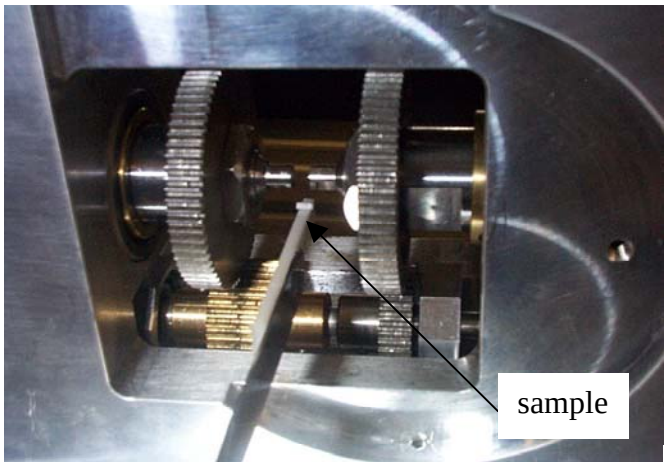

Figure 7.3: Photograph of the scaffold being placed between the grips of the tomopress at ESRF's ID 22.

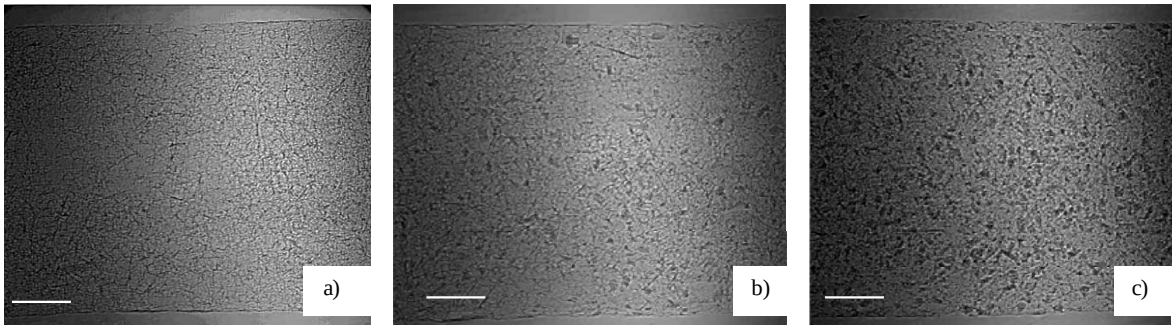

Figure 7.4: Phase contrast X-ray radiographs of the degradable scaffolds, a) PLA without glass, b) PLA with 20 wt% of glass particles, and c) PLA with 50 wt% of glass particles. (Scale bars represent 200μm)

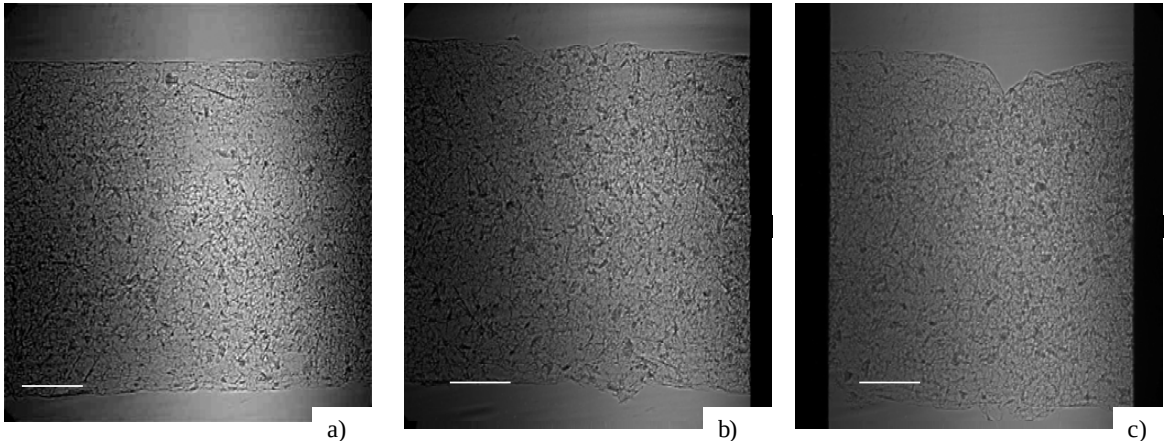

Figure 7.5: Phase-contrast X-Ray radiographs at different strain levels : a) 0%, b) 20% and c) 50%. The solid black lines at the edges of the images are the tomopress grips. (Scale bars represent 200μm)

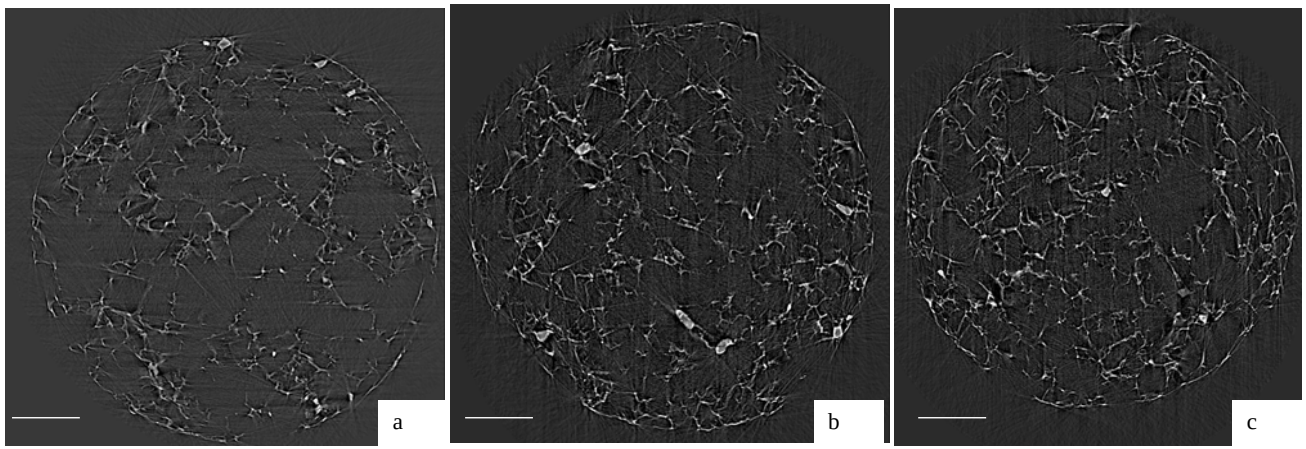

Figure 7.6: 2D slices of a scaffold with 20 wt% of glass particles at different strain levels: a) 0% strain, b) 20% strain and c) 40% strain. (Scale bars represent 200μm)

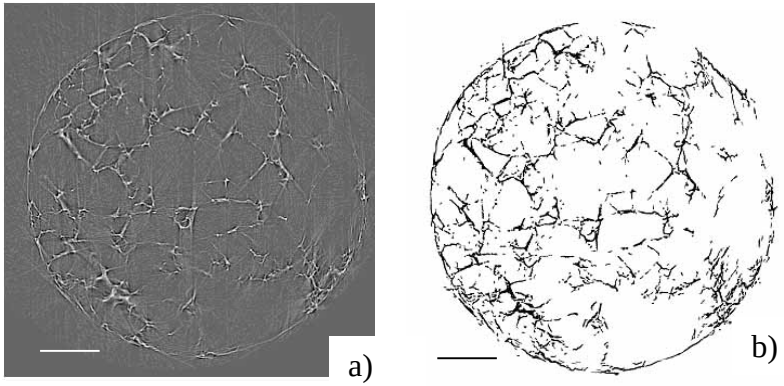

Figure 7.7: Reconstructed slices of a scaffold with 0wt% of glass: a) before image treatment, and b) after image treatment to reduce noise by thresholding and particle removal. (Scale bars represent 200 μm)

The stacks of X-ray radiographs were reconstructed into 2D slices which further illustrated scaffold microstructure. These slices reveal the densification of scaffold material, namely glass particles, as the structure become more and more compressed (Figure 7.6). The high levels of noise in the 2D slice images can be greatly reduced by generating binary images (images in black and white only). Binary images are created by thresholding the image, thus separating matter from air. After thresholding, a particle removal function was applied in order to eliminate noise which had been included in the thresholding, similarly to what Müller et al [5] report (Figure 7.7).

The binary images of the slices were in turn reconstructed into 3D images that give a comprehensive picture of the scaffold microstructure and follow pore deformation under compression in 3D. Figure 7.8 shows the 3D images highlighting the deformation of a pore within the structure during compression. The image treatments used to clean the image of noise do not significantly alter their content as can be seen for the comparison between SEM images and 3D reconstructions in Figure 7.10.

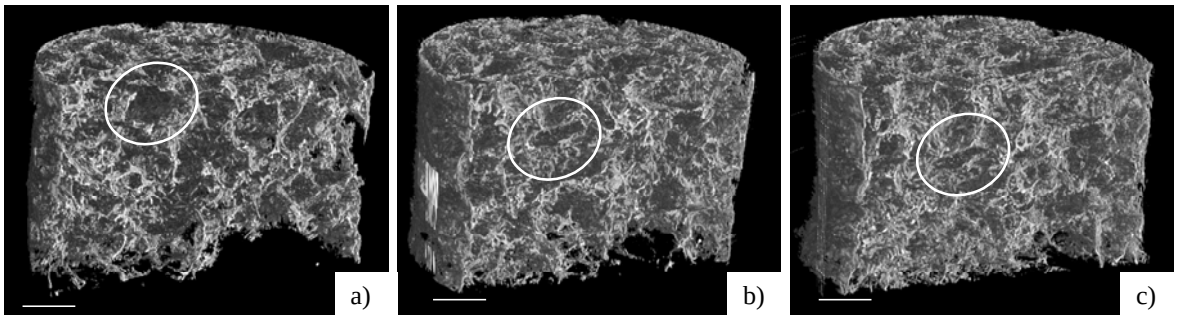

Figure 7.8: Three-dimensional images of the microstructure of the scaffolds at different strain levels: a) 0% strain, b) 10% strain and c) 30% strain. (Scale bars represent 200 μm)

The 3D reconstructions can be used to quantify some porosity parameters. The porosity of the scaffolds calculated using these binary images was 94% for all compositions (Table 7.1). Converting the slices into binary images, however, eliminates information on the phases of the composite material; the PLA and glass particles are undistinguishable. Thus, the slices were also treated as greyscale images, thresholded (without particle removal) and used to study the glass distribution within the structure. The porosity and volume percent of the phases of each composition calculated using the greyscale images are shown in Table 7.1 and Table 7.2.

Weight % Glass	Porosity (experimental)	Porosity (binary image analysis)	Porosity (greyscale image analysis)
0%	95%	94%	88%
20%	95%	94%	86%
50%	95%	94%	86%

Table 7.1: Values of porosity calculated for the different compositions using experimental and image treatment techniques.

Weight % of glass	Volume% of polymer (theoretical)	Volume% of polymer (image analysis)
0%	100%	/
20%	90.4%	86.9%
50%	70.2%	77.5%

Table 7.2: Volume percent of glass particles in the scaffolds calculated theoretically from the weight % and by image analysis.

The 3D images can also be analysed in order to quantify pore interconnectivity and surface/volume ratios. Similarly to what Darling and Sun [23] report, the pore interconnectivity calculated using the region-growing function gave interconnectivities of more than 99% for all compositions. The surface/volume ratio of the scaffolds is in the order of 1000 mm^2/mm^3 for all compositions. Qualitatively the greyscale images illustrate the 3D distribution of the glass particles within the porous scaffold structure (Figure 7.9). These images also confirm the uniform distribution of the glass particles seen previously in the projections (Figure 7.4).

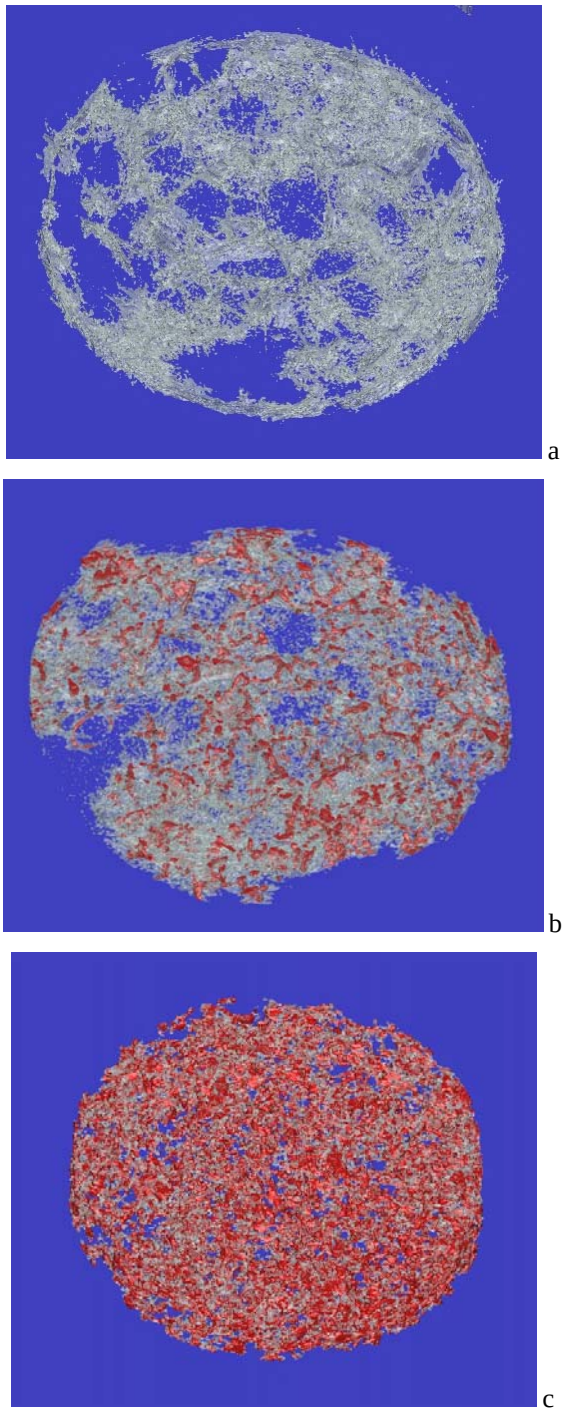

Figure 7.9: 3D images of the microtomographical reconstructions of the scaffold with a) only PLA (in translucent white), b) 20wt% of glass particles (in solid red) and c) 50 wt% of glass particles.

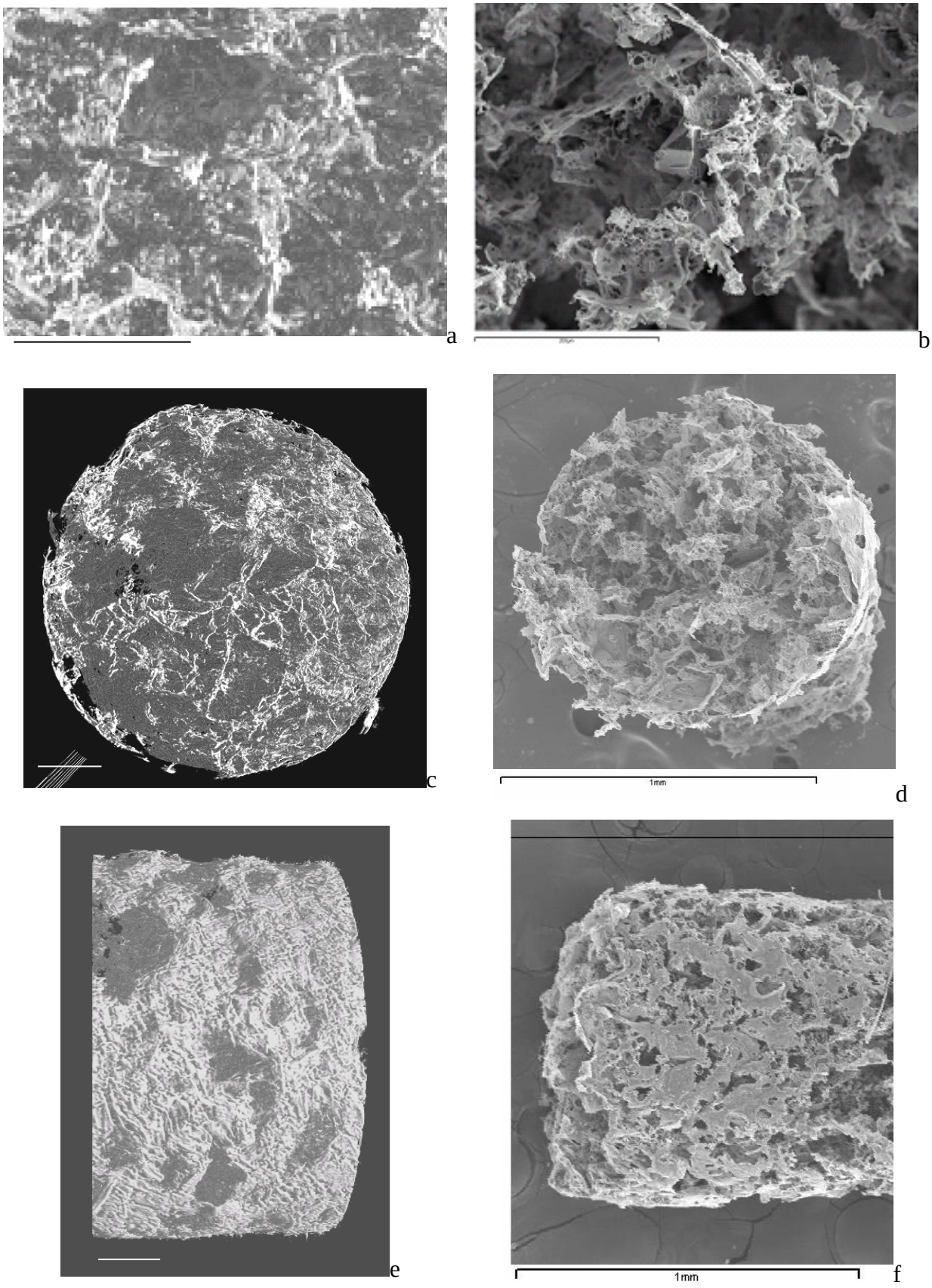

Figure 7.10: Comparison between the microtomography images (left) and SEM images (right). All samples are cylindrical and measure approximately 1.2 mm in diameter. (Scale bars for microtomography images (left) represent 200 μm)

Finite Element Analysis

The 3D volume images were converted into a surface mesh of triangular elements using Mimics (Materialise software). The Magics (Materialise software) module was then used to correct the mesh by reducing the number of triangles and increasing triangle quality in order to be able to create a correct volume mesh. The surface mesh was then exported to the Mentat (MSC software) pre-processor and meshed in volume with tetrahedral elements. This finite element model of a scaffold was used to perform a simulation in order to validate the accuracy of the model. A simulation of a compression test at 5% strain was performed using Marc (MSC software). The nodes on the lower surface of the scaffold were fixed with no displacement nor rotation. The nodes on the upper surface were assigned a fixed displacement of 7μm down (in the negative z direction) which corresponded to 5% strain of the model (Figure 7.11).

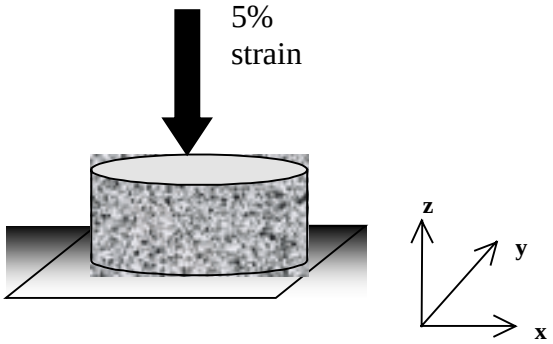

Figure 7.11: Schematic illustration of the simulation of a compression test performed to validate the scaffold finite element model

The 5% strain simulation on the scaffold model converged and its results were analysed in order to validate the model. The total reaction force due to the compression, F_{num}, was 0.0218N, which gave a stiffness, k_{num}, of 3120 N/m as computed using:

$$k_{num} = \frac{F_{num}}{\Delta l} \qquad \{2\}$$

where, Δl is the displacement of the scaffold.

The experimental value of the stiffness, k_{exp}, was 2172 N/m, as calculated using:

$$k_{\exp} = \frac{E_{\exp}}{l \times A} \qquad \{3\}$$

where, E_{exp}, is the Young's Modulus obtained from compression tests of the macroscopical samples, l is the length (or height in this case) of the scaffold, and A is the surface area of the upper surface of the scaffold.

The results of the simulation were also used to obtain a preliminary analysis of the stress and strain distribution in the model. The distribution of the major principal stress throughout the scaffold, shows the stress is concentrated on the corners of pore walls and especially on thin pore walls. The distribution of the major principal elastic strain, shows that most of the scaffold undergoes about 5% strain, though some pore walls are submitted to up to 15% strain. The shear strain in the scaffold was generally below 1% and the maximum von Mises stress was approximately 300 kPa (Figure 7.12).

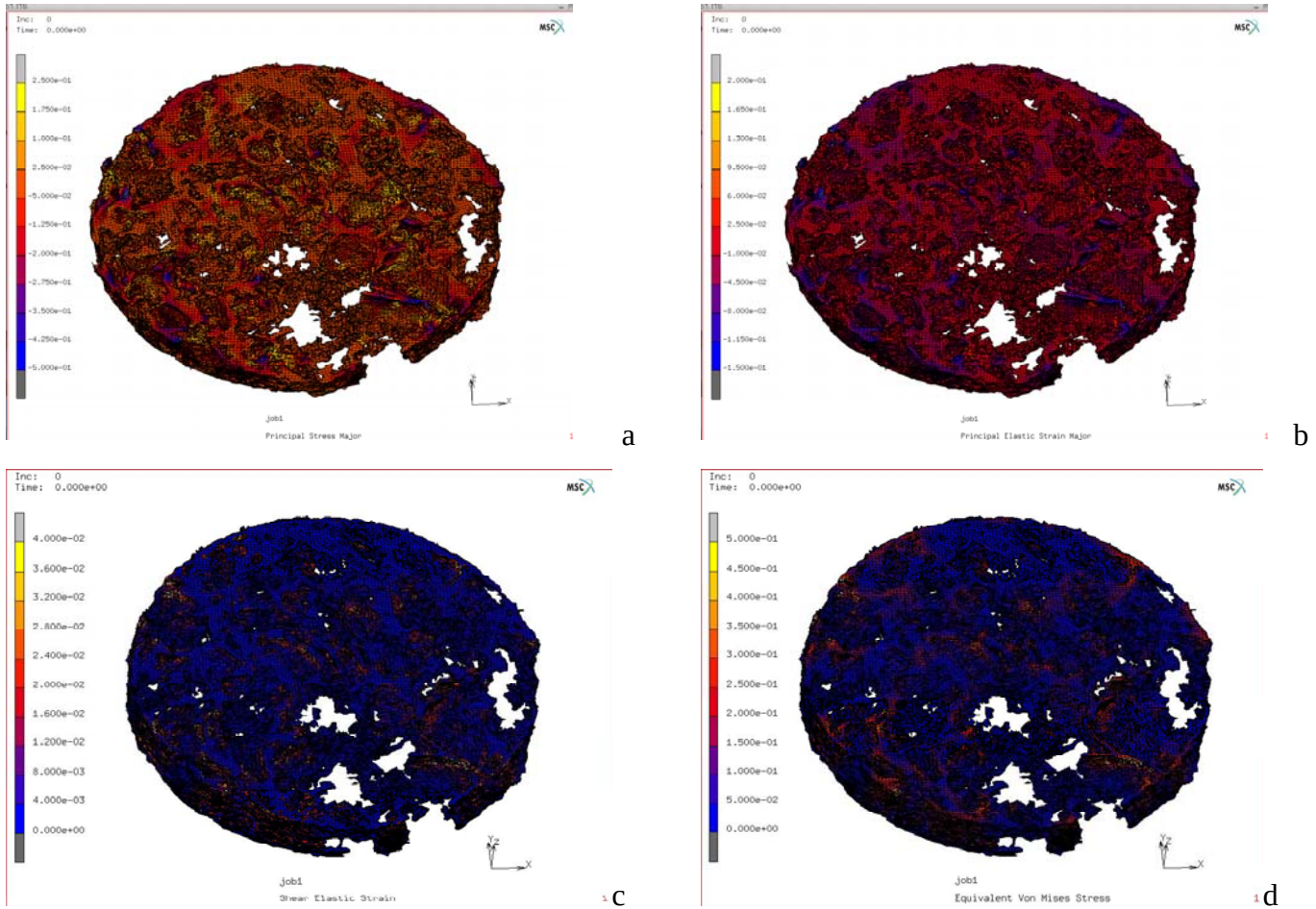

Figure 7.12: Distribution of some values of stress and strain throughout the scaffold structure after the simulation of a compression with 5% strain; a) Major principal stress, b) Major principal elastic strain, c) Shear elastic strain and d) equivalent von Mises stress

Discussion

This experiment with synchrotron X-ray microtomography confirms the enormous potential this tool can have in the field of tissue engineering characterisation. As has been discussed in the introduction of this chapter, this tool can also be used to study the scaffold-cell construct after cell culture, and thus characterise the scaffold during its entire working life. In the case of the solvent cast scaffolds, synchrotron X-ray microtomography has allowed for a complete qualitative and quantitative survey of scaffold properties in 3D, and has provided a finite element model which will be used for extended numerical analysis[24].

The 3D images and projections obtained with the microtomography experiment confirm the high porosity and homogeneous distribution of glass particles within the scaffolds. The glass distribution cannot be visualised without 3D imaging techniques. The images also give qualitative confirmation of pore interconnectivity and of the deformation of the material under compression.

Binary image treatments allow the analysis of low-noise images whose porosity values conform to those measured by mercury pycnometry (Table 7.1). The porosities calculated with the greyscale images tend to underestimate the real porosity of the scaffolds due to the inclusion of the noise in the volume of the masks. In fact, the composition with 50wt% of glass produces especially noisy tomographies. The effect of the noise could also explain the divergence between the theoretical and the image analysis Vol% values (Table 7.2). These differences could also be due to the errors in thresholding which would overestimate the volume of one phase or another. Pore interconnectivity values are very high and confirm the properties of the scaffolds one would expect due to their high porosity and permeability. The quantitative evaluation of the interconnectivity of the scaffolds has been an ongoing challenge in the field of tissue engineering [25]. The scaffolds have very high surface/volume ratios, as compared to that of trabecular bone for example: 20 mm^2/mm^3 [26]. This should ensure large areas for cell attachment, and nutrient and waste transport within their structure.

In general, all quantitative values computed from the images are within an appropriate range but must be interpreted with caution due to some uncertainties introduced by thresholding and noise reduction. The analysis of both binary and

greyscale images helps understand the possible limitations of each method and should be considered complementary.

The finite element model of the composite scaffold developed from the microtomographical images has been validated by comparing the results between the stiffness of the scaffold as calculated with the compression simulation, and the experimental value found in previous compression tests. k_{num} and k_{exp} give values of 3120N/m and 2172N/m respectively, which are in the same order of magnitude. The differences between the numerical and experimental stiffnesses may be due to the value of 3.5 MPa chosen as the stiffness of the solid composite material. This value was derived empirically using equation [2], with values of stiffness associated to compression tests whose accuracy is limited as discussed in the introduction. Furthermore, the finite element model corresponds to a section of a single scaffold, thus including its singularities and possible errors introduced during the tomographical scan, the image treatment and the meshing. Despite these limitations, the accordance between the numerical and experimental values is clear, and is an exciting first step towards the characterisation of the scaffolds by means of finite element analysis.

Indeed, an accurate, validated finite element model could be used as a complementary approach to conventional mechanical tests. This would allow for the detailed study of the stresses and strains developed in the scaffold, without the limitations of friction hills, sample buckling and other problems associated to the nature of tissue engineering materials [27]. The compressed models can be compared to the microtomographies of the scaffolds under compression in order to further validate and adjust the model. In addition to evaluating their overall mechanical properties, the finite element analysis will illustrate the micromechanical environment the cells will sense after being seeded in the scaffolds and could predict tissue growth under certain biomechanical conditions. Future improvements of the model will include the modelling of a biphasic material, studying the contact between the glass particles and the polymer.

This experiment was thus a successful first contact with in-situ mechanical tests combined with synchrotron X-ray microtomography. Both performing the experiment and analysing the data proved very challenging due to the enormous amount of data that generated: more than 1 terabyte (10^{12}), of information. The size of the files made all steps of the image treatment slow and the files were often divided in order to deal with

more complex operations. Despite this fact, very useful qualitative and quantitative information was derived from this experiment. There were, however, two main limitations to its scope. One limitation was due to the low contrast between the polymer and glass phases which make image treatment complex. The images and their translation into finite element meshes should thus be interpreted with caution. Another limitation of the study was the fact that a small but unknown amount of pre-strain was applied to the samples in order to grip them in the tomographical press, this was due to the fact that the press was not optimised for these materials. Both issues are being addressed at present.

Conclusions

- This experiment is the first time synchrotron X-ray microtomography had been combined with in-situ micromechanical tests to characterise porous scaffolds for Tissue Engineering
- This first contact with synchrotron X-ray microtomography was challenging but has been an exciting first step towards this type of characterisation which holds enormous potential
- The 2D projections and radiographs confirm pore interconnection, both quantitatively and qualitatively. This has been an ongoing challenging in Tissue Engineering science.
- Image treatment allows for very graphical visualisation of glass distribution, pore morphology and pore deformation under compression.
- The accuracy of the image treatment has been confirmed by the porosity readings, the comparison with SEM images and by the validation of the finite element model.
- The validated finite element model could be used to characterise the scaffolds' mechanical properties in detail, to study the microenvironment seeded cells will sense and to study the scaffolds in bioreactor conditions.

Publications

The results of this study have been published in:

"Mechanical and structural characterisation of completely degradable polylactic acid/calcium phosphate glass scaffolds"
M.Charles-Harris, S. del Valle, E.Hentges, P.Bleuet, D.Lacroix, J.A.Planell
Biomaterials 2007, vol 28, pp 4429-4438

Acknowledgements

We acknowledge the European Synchrotron Radiation Facility for the beamtime and Dr. Pierre Bleuet for his technical support during and after the tomography experiment.

Bibliography

(1) Wiedemann H. Synchrotron Radiation. Springer-Verlag Berlin 2003.

(2) European Synchrotron Radiation Facility (ESRF). A light for Science. www.esrf.fr . 2007.

(3) Rustichelli F, Romanzetti S, Dubini B, Girardin E, Raven C, Snigrev A, Rizzi G. Phase-contrast microtomography of thin biomaterials. J Mater Sci Mater Med 2004; 15:1053-1057.

(4) Maspero FA, Ruffieux K, Müller B, Wintermantel E. Resorbable defect analog PLGA scaffolds using CO_2 as solvent: Structural characterization. J,Biomed Mater Res 2002; 62:89-98.

(5) Müller B, Beckmann F, Huser M, Maspero FA, Székely G, Ruffieux K, Thurner P, Wintermantel E. Non-destructive three-dimensional evaluation of polymer sponge by micro-tomography using synchrotron radiation. Biomolec Eng 2002; 19:73-78.

(6) Gauthier O, Khairoun I, Bosco J, Obadia L, Bourges X, Rau C, Magne D, Bouler JM, Aguado E, Daculsi G, Weiss P. Noninvasive bone replacement with a new injectable calcium phosphate biomaterial. J,Biomed Mater Res 2003; 66A:47-54.

(7) Weiss P, Obadia L, Magne D, Bourges X, Rau C, Weitkamp T, Khairoun I, Bouler JM, Chappard D, Gauthier O, Daculsi G. Synchrotron X-ray microtomography (on a micron scale) provides three-dimensional imaging representation of bone ingrowth in calcium phosphate biomaterials. Biomaterials 2003; 24(25):4591-4601.

(8) Mastrogiacomo M, Komlev VS, Hausard M, Peyrin F, Turquier F, Casari BS, Cedola A, Rustichelli F, Cancedda R. Synchrotron Radiation Microtomography of Bone Engineered from Bone Marrow Stromal Cells. Tissue Eng 2004; 10(11/12):1767-1774.

(9) Thurner P, Müller B, Raeber G, Sennhauser U, Hubbell JA. 3D Morphology of Cell Cultures: A Quantitative Approach using Micrometer Synchrotron Light Tomography. Microscopy Res Tech 2005; 66:289-298.

(10) Tuan HS, Hutmacher DW. Application of micro CT and computation modeling in bone tissue engineering. Computer-Aided Design 2005; 37:1151-1161.

(11) Marra KG, Szem JW, Kumta PN, DiMilla PA, Weiss LE. In Vitro Analysis of Biodegradable Polymer Blend/Hydroxyapatite Composites for Bone Tissue Engineering. J,Biomed Mater Res 1999; 47:324-335.

(12) Xiong Z, Yan Y, Wang S, Zhang R, Zhang C. Fabrication of Porous Scaffolds for Bone Tissue Engineering Via Low-Temperature Deposition. Scripta Materialia 2002; 46:771-776.

(13) Hou Q, Grijpma DW, Feijen J. Porous Polymeric Structures for Tissue Engineering Prepared by Coagulation, Compression Moulding and Salt Leaching Technique. Biomaterials 2003; 24:1937-1947.

(14) Zhang R, Ma PX. Poly(α-Hydroxyl Acids)/Hydroxyapatite Porous Composites for Bone Tissue Engineering. I. Preparation and Morphology. J,Biomed Mater Res 1999; 44:446-455.

(15) ASTM D 1621-00 Standard Testing Method for Compressive Properties of Rigid Cellular Plastics. 2000.

(16) ASTM D695-96 Standard Testing Method for Compressive Properties of Rigid Plastics. 1996.

(17) ASTM F451-99a Standard Specification for Acrylic Bone Cement. 1999.

(18) Somogyi A, Tucoulou G, Martinez-Criado G, Homs A, Cauzid J, Bleuet P, Bohic S, Simionovici A. ID22: a multitechnique hard X-ray microprobe beamline at the European Synchrotron Radiation Facility. J, Synch Rad 2005; 12:208-215.

(19) Natterer F, Wübbeling F. Mathematical Methods in Image Reconstruction. Philadelphia: Society for Industrial and Applied Mathematics, 2001.

(20) Bleuet P, Boivin G, Roux J-P, Dabin Y. In-Situ Micro-Tomography study of Human Bones under Strain with Synchrotron Radiation. SPIE Devlopments in X-Ray Tomography IV, Denver 2004; 5535:129-136.

(21) Lin AS, Barrows TH, Cartmell SH, Guldberg RE. Microarchitectural and mechanical characterization of oriented porous polymer scaffolds. Biomaterials 2003; 24(3):481-489.

(22) Gibson LJ, Ashby MF. Cellular Solids, Structure and Properties. second ed. Cambridge: Cambridge University Press, 1997.

(23) Darling AL, Sun W. 3D microtomographic characterization of precision extruded poly-epsilon-caprolactone scaffolds. J Biomed Mater Res B Appl Biomater 2004; 70(2):311-317.

(24) Charles-Harris M, del Valle S, Hentges E, Bleuet P, Lacroix D, Planell JA. Mechanical and Structural characterisation of completely degradable polylactic acid/calcium phosphate glass scaffolds. Biomaterials. In press.